Journal of Power Sources 342 (2017) 165–174

Contents lists available at ScienceDirect

Journal of Power Sources

journal homepage: www.elsevier.com/locate/jpowsour

Application of electrospun CN_x nanofibers as cathode in microfluidic fuel cell

Amandeep Jindal [a], Suddhasatwa Basu [a, *], Neha Chauhan [b], Tomofumi Ukai [b], D. Sakthi Kumar [b], K.T. Samudhyatha [c]

[a] Department of Chemical Engineering, Indian Institute of Technology Delhi, New Delhi 110016, India
[b] Bio-Nano Electronics Research Centre, Toyo University, Kawagoe, Saitama, 350-8585, Japan
[c] Department of Physics, Indian Institute of Science, Bangalore 560012, India

HIGHLIGHTS

- Microfluidic fuel cell (MFC) with active area of 0.11 cm^2 is fabricated.
- Formic acid is used as fuel and $KMnO_4$ as oxidant for MFC operation.
- CN_x nanofibers as cathode catalyst exhibits maximum power density of 3.43 mW cm^{-2}.
- CN_x nanofibers power density comparable to Au (2.72 mW cm^{-2}), Pt (3.09 mW cm^{-2}).
- MFC power density at flow rate of 300 μL min^{-1} higher against 400 and 500 μL min^{-1}.

GRAPHICAL ABSTRACT

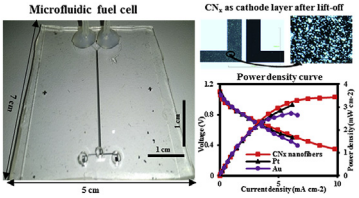

ARTICLE INFO

Article history:
Received 13 October 2016
Received in revised form
26 November 2016
Accepted 12 December 2016

Keywords:
Microfluidic fuel cell
Cathode catalyst
Carbon nitride nanofibers
Formic acid

ABSTRACT

Carbon nitride (CN_x) nanofibers is successfully utilised as cathode catalyst in microfluidic fuel cell (MFC) using electrospinning technique. The electrochemical measurement for CN_x nanofibers as cathode catalyst in MFC is studied and compared with that of Pt and Au cathodes. Formic acid is employed as fuel, $KMnO_4$ as oxidant and H_2SO_4 as supporting electrolyte. CN_x nanofibers is shown to be not active towards formic acid oxidation and as a result, is tolerant to fuel crossover effect as compared to Pt and Au cathode. CN_x nanofibers enable MFC to operate at a wider range of flow rates of fuel and oxidant as compared to Pt and Au conventionally used. MFC utilising CN_x nanofibers gives higher power density of 3.43 mW cm^{-2} and the current density of 9.79 $mAcm^{-2}$, as compared to that utilizes pure Au (2.72 mW cm^{-2}, 6.04 mA cm^{-2}) and Pt (3.09 mW cm^{-2}, 6.18 mA cm^{-2}) as anode.

1. Introduction

Recent increase in demand of power source for portable devices, that include common devices such as mobile phones to specialised devices such as clinical diagnostic tests, have increased momentum in research for microfluidic fuel cells (MFC) [1,2]. MFC operates without a physical barrier as the liquid fuel and oxidant maintain laminar flow regime within microfluidic channel [3–5]. Normally proton exchange membrane (PEM) is used as the solid electrolyte, which maintains a barrier between anolyte and catholyte and allows proton transfer in the case of PEM fuel cell. However, Dector et al. [3] showed that MFC can be used without using PEM by

* Corresponding author.
E-mail address: sbasu@iitd.ac.in (S. Basu).

http://dx.doi.org/10.1016/j.jpowsour.2016.12.047
0378-7753/

maintaining a co-laminar flow of anolyte and catholyte and keeping mixing zone at the interface minimum.

Most of the MFC developed till date utilizes Pt or Pt-based material as cathode catalyst [5,6]. However, Pt being expensive, hampers the commercial viability of the MFC. In order to boost the commercial viability of MFC, cathode catalysts are widely studied that replaces Pt catalysts [1,7,8]. Gago et al. observed that MFC that uses carbon-supported ruthenium chalcogenide as cathode catalyst showed better maximum power density (1.97 mW cm^{-2}) than Pt/C catalyst (1.89 mW cm^{-2}), boosting the research prospects in carbon-based materials as cathode catalyst [9]. Carbon nitride (CN_x), a nitrogen-containing carbon material, has been reported to show good activity as oxygen reduction reaction (ORR) catalyst [10–12]. In the previous discourse of our studies, electrospun carbon nitride (CN_x) nanofibers are studied that exhibited ORR activity comparable to Pt/C catalysts [13–15]. Electrospun CN_x/PAN nanofibers, incorporated with carbon black and Nafion® fillers, (referred as CN_x nanofibers) showed comparable onset potential (0.95 V) and peak current density (6.32 mA cm^{-2}) compared to that of Pt/C catalysts (0.97 V, 6.41 mA cm^{-2}) in voltammetry studies for ORR [14]. In the present study, CN_x nanofibers is used as electrocatalyst for $KMnO_4$ reduction, the cathode reaction of MFC. Furthermore, CN_x nanofibers is successfully laid in the cathode channel of the MFC using electrospinning technique coupled with lift-off, improving its maximum power density achieved as compared to Pt catalyst. Fuels like formic acid, methanol and ethanol are not active to CN_x nanofiber. Thus, use of CN_x nanofibers, being tolerant to fuel crossover, as cathode catalyst allows lower flow rate operation of MFC without jeopardizing efficiency of power generation.

Formic acid is preferred as fuel due to its considerable advantages over other fuels, such as methanol, ethanol and hydrogen. It has higher overall theoretical open circuit potential (1.48 V) as compared to hydrogen (1.23 V) and methanol (1.21 V) [5]. Moreover, it acts as both fuel and the proton conductor in the MFC [16]. Choban et al. observed that when potassium permanganate is employed as the oxidant in formic acid MFC, it exhibited one order of magnitude higher current density and power density (4 mA cm^{-2}, 2.4 mW cm^{-2}) as compared to that when oxygen saturated stream is used as oxidant (0.4 mA cm^{-2}, 0.17 mW cm^{-2}). Moreover, potassium permanganate as the oxidant gives high cell potential due to its high reduction potential (1.7 V) as compared to O_2 as oxidant [17]. Previous literature suggests that gold layer can be used as current collector due to its stability and good electrical conductivity [6,18].

In the present study, CN_x nanofiber is utilised as the cathode catalyst for formic acid MFC, fabricated based on the design as shown in Fig. 1. Platinum is used as anode layer for all the studies. The gold layer is used as the current collector and the titanium layer is used as the adhesion layer. The performance of MFCs with different cathode catalysts, e.g., CN_x, Pt, Au, are compared at different flow rates. The liquid fuel (formic acid) and oxidant (potassium permanganate), mixed with the liquid electrolyte (sulphuric acid), are fed in a Y-shaped MFC. The interfacial layer of the fuel and the oxidant flow in the microchannel of MFC comprising CN_x nanofiber, Pt and Au as cathode catalyst is visually observed and current-voltage characteristics are compared and analysed with the variation of flow rates of fuel and oxidant.

2. Experimental section

2.1. Fabrication of microfluidic fuel cell

MFC presented in this work is composed of the glass slide containing patterned electrodes and the Y-shape microchannel made of PDMS, which is used to introduce the fuel and the oxidant. The fabrication steps are presented in Fig. S1 of the supplementary information. Initially, a glass slide (70 mm × 50 mm) was coated with two positive photoresists, LOR 20B (Microchem Corp., Newton, M.A) and OFPR-800 LB (Tokyo Ohka Kogyo, Japan). The LOR resist helps in easy lift-off of the metals due to the prominent undercut created beneath the LOR resist. UV-lithography (Karl Suss, MA6) was used to define the anode coating area (Fig. S1 (a)) and NMD-3 developer (2.38%, Tokyo Ohka Kogyo) was used to create undercut resist patterns for the deposition of metal electrodes. The glass slide was then coated with Ti (10 nm), as an adhesion layer, and Pt (50 nm) using EB evaporator system (ULVAC, EX-550-D10), followed by lift-off process using PG remover (Microchem Corp., Newton, M.A) (Fig. S1 (b)) to define the shape of the anode. Subsequently, cathode coating area was defined on the same glass slide using mask aligner and UV-lithography (Fig. S1 (c)). The anode and cathode catalyst films are placed parallel at the separation of 100 μm. The resultant glass slide was deposited with cathode followed by the lift-off process using PG remover (Fig. S1 (d)). For the cathode, firstly Ti layer (10 nm) was deposited as the adhesion layer, followed by Au layer (50 nm), as the current collector layer. CN_x nanofibers cathode catalyst was synthesized using electrospinning (NANON-01A, MECC Co., Ltd., Fukuoka, Japan) in the same way, as explained in our previous study [14], keeping the glass slide (EB deposited with Ti (10 nm), Au (50 nm)) as the collector during electrospinning. MFC activity utilising CN_x nanofibers catalyst is compared with that using Pt (50 nm) and Au (50 nm) as the cathode, keeping the Ti (10 nm) as adhesion layer underneath.

In order to synthesize CN_x nanofibers, firstly CN_x nanoparticles were synthesized using ethylenediamine (Merck) and carbon tetrachloride (Merck) as precursors. Ethylenediamine and carbon tetrachloride were mixed, refluxed in a nitrogen atmosphere at 90 °C for 6 h and then calcined in the nitrogen atmosphere for 5 h at 600 °C. Electrospinning of the resultant CN_x nanoparticles was performed using polyacrylonitrile (Average molecular weight: 1,50,000, Sigma-Aldrich) and dimethyl formamide (DMF, Kanto Chemical Co., Inc.). Dispersion of 5% (w/v) CN_x nanoparticles in 5% (w/v) PAN/DMF solution was prepared. Carbon black powder Vulcan XC-72 R (GP-3919, Cabot) (1% (w/v)) was added in the prepared solution. After drying 2 mL of Nafion® dispersion (DE-521, DuPont, USA) at 80° C, it was added to 10 mL of the prepared solution. Electrospinning was carried out at 30 kV voltage and flow rate of 0.5 mL h^{-1} maintained by a syringe pump as per formulation in electrospinning unit. Surface morphology and size of CN_x nanofibers were analysed using TEM (Jeol JEM 2200-FS) and SEM (Hitachi SEM SU8030). The effect of PG remover (used for lift-off) on CN_x nanofibers was studied by carrying out SEM of CN_x nanofibers after treating it with PG remover. X-ray photoelectron spectroscopy (XPS) (PHI Quantes, Scanning Dual X-ray Photoelectron Microprobe, ULVAC-PHI, INC) was performed to study the characteristic absorption peaks of the CN_x nanofibers, before and after treating with PG remover. XPS was performed under a basic pressure of 10^{-7} - 10^{-8} Torr. The X-ray source used was anode Al with the pass energy of 240 eV for wide spectrum and 140 eV for individual spectra. The XPS data fitting was performed using MultiPak software.

The electrocatalytic activity of CN_x nanofibers towards $KMnO_4$ reduction was studied by linear sweep voltammetry (LSV) using three-electrode cell assembly connected to potentiostat-galvanostat (PGSTAT 128 N, AUTOLAB). Ag/AgCl (in saturated KCl) electrode, Pt wire and H_2SO_4 (0.5 M) mixed with $KMnO_4$ (0.144 M) were used as reference, counter electrode and electrolyte

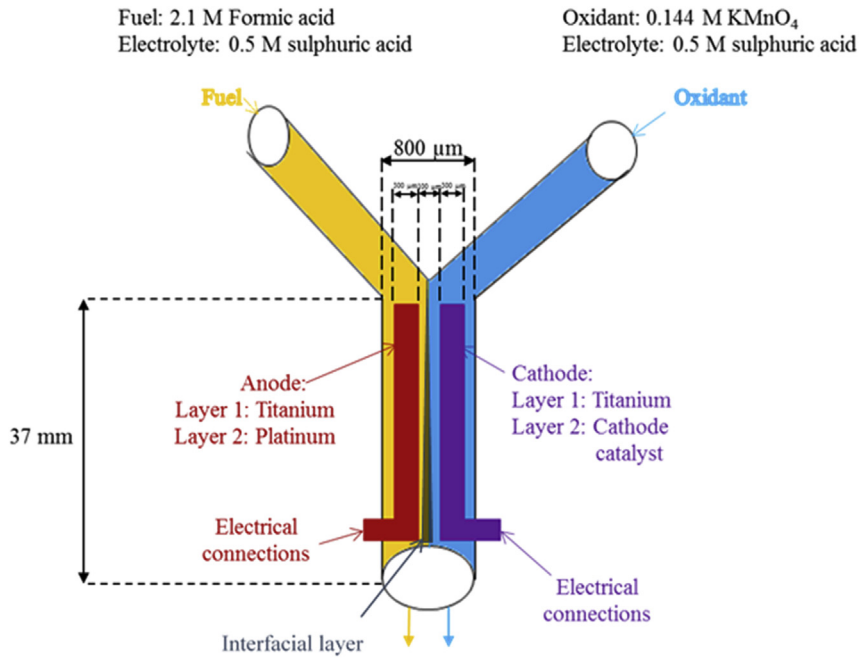

Fig. 1. Y-shaped microfluidic fuel cell with microchannel of dimensions 800 μm (W) × 125 μm (H) x 3.7 cm (L); anode (width 300 μm) and cathode (width 300 μm). Distance between the electrodes 100 μm such that interfacial layer lies within this region.

respectively. All the potential values measured are relative to reversible hydrogen electrode (RHE). The working electrode was prepared using CN_x nanofibers as catalyst material. Twenty milligram of the catalyst was ultrasonicated in 4 mL isopropanol and 40 μL Nafion® dispersion for 1 h to prepare the catalyst ink. The prepared catalyst ink was dropped on to 1.6 mm diameter circular glassy carbon electrode and dried at room temperature. The catalyst loading of 1 mg cm^{-2} was used. LSV for $KMnO_4$ reduction was carried out on CN_x nanofibers and bare glassy carbon electrode at the scan rate of 20 mV s^{-1}. LSV on CN_x nanofibers was carried out over 1000 repetitions at the scan rate of 20 mV s^{-1} to study the stability of CN_x nanofibers in $KMnO_4$ environment. LSV on CN_x nanofibers in 0.5 M H_2SO_4 + 0.144 M $KMnO_4$ (1:1 volumetric ratio) solution was compared with LSV in 0.5 M H_2SO_4 + 0.144 M $KMnO_4$ + 2.1 M HCOOH (1:1:1 volumetric ratio) solution to understand the formic acid crossover effect. The cyclic voltammetry (CV) on Pt, Au and CN_x nanofibers towards $KMnO_4$ reduction is performed to understand the electrochemical transition of Mn ions. The detailed CV procedure is provided in the supplementary information.

In order to fabricate the microchannel, polydimethylsiloxane (PDMS, TSE 3450, Momentive Performance Materials Inc., USA) was used. Firstly, the master template defining the shape of the microchannel was prepared using the SU-8 photoresist (SU-8 3050, Microchem Corp., Newton, M.A.). The master was the SU-8 photoresist pattern defined by UV-lithography on the silicon wafer (Fig. S1 (e)). The dimensions of the microchannel were 800 μm (W) x 125 μm (H) x 37 mm (L). Subsequently, the PDMS prepolymer and the curing agent mixed in the ratio of 1:10 were poured onto the master template followed by degassing in a vacuum desiccator for 1 h (Fig. S1 (f)). After curing the degassed PDMS at room temperature for 6 h, it was peeled off from the master template (Fig. S1 (g)). The holes were punched in the PDMS microchannel for the inlets, outlet and for taking the electrode connection. Finally, the PDMS microchannel was aligned using the alignment marks and soft-bonded with metallized glass slides so that the electrodes lie within the microchannel width (Fig. S1 (h)).

The assembled MFC was analysed using Nikon Eclipse LV100 optical microscope with a digital camera (Nikon Digital Sight DS-Fi1). Fig. 2 (a) shows the assembled MFC and the microscopic images of Y-junction and mid part of the MFC with the electrodes are shown in Fig. 2 (b) and 2 (c). It may be noted that no plasma bonding or UV vacuum process was needed to bond the microchannel and the glass slide and the assembled MFC was able to withstand the flow rates up to 1 mL min^{-1}. The active surface area was calculated to be 0.11 cm^2.

2.2. Flow interfacial studies and MFC activity measurements

Fuel was prepared by mixing 0.5 M H_2SO_4 (98%, Kanto Chemical Co., Inc.) and 2.1 M HCOOH (98%, Nacalai Tesque, Inc.) in the ratio of 1:1. Oxidant was prepared by mixing 0.5 M H_2SO_4 and 0.144 M $KMnO_4$ (Kanto Chemical Co., Inc.) in the ratio of 1:1. Pressure driven fluid flow was incorporated in all MFC tests, the flow rates of which were regulated by the syringe pump (KD Scientific Inc.). The flow rates of the fuel and the oxidant were kept same and in the range of 50–500 μL min^{-1}. The fluid flows through the microchannel was analysed using the microscope (Nikon Instech Co., Ltd., TE2000-U) with high-speed CCD camera (DS-2Mv, Digital Sight). The width of the interfacial layer of the fuel and the oxidant flow in the microchannel was calculated by studying the flow profile of the fluid interface in the microchannel using ImageJ software version 1.48 (NIH, USA). The electrical connections from the electrodes were taken through the tungsten probes. Current-voltage measurements were performed using the semiconductor device analyser (Agilent Technology B1500A). MFC setup during cell testing and its schematic are shown in Fig. 3 (a) and Fig. 3 (b) respectively.

3. Results and discussions

3.1. CN_x nanofibers as cathode catalyst

CN_x nanofibers are electrospun directly on the glass slide, after gold deposition using EB evaporator. Polyacrylonitrile (PAN) is used

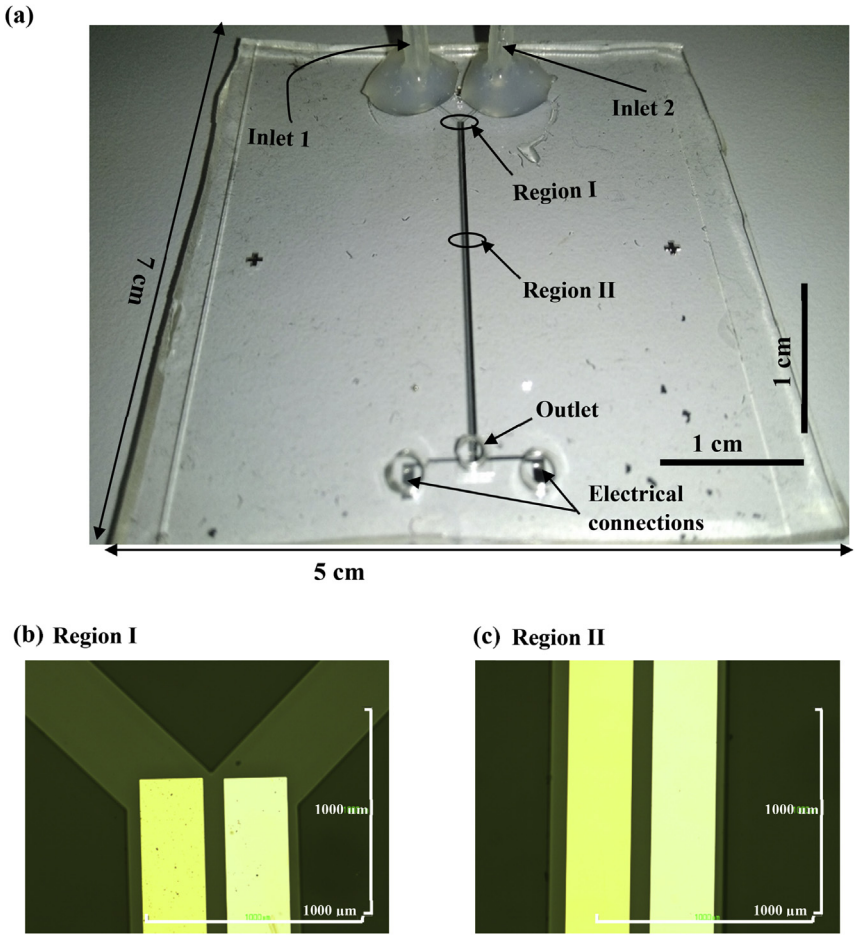

Fig. 2. (a) Assembled microfluidic fuel cell; Microscopic images (b) Y-junction of the microchannel (region I in Fig. 2 (a)) and (c) the middle part of the microchannel (region II in Fig. 2 (a)). Left electrode is gold cathode and right electrode is platinum anode patterned on glass surface.

as supporting polymer and carbon black and Nafion® dispersion as fillers. SEM and TEM image of CN_x nanofibers are shown in Fig. S2 (a) and Fig. S2 (b) respectively of the supplementary information. The average size of CN_x nanofibers is observed from SEM as 75 nm. TEM micrograph shows that CN_x is dispersed as a layer on PAN nanofibers. The stability of CN_x layer is attributed to the binding property of Nafion® dispersion. In some cases, CN_x nanoparticles, supported on carbon black, are observed to be dispersed in PAN nanofibers as nodes, which is discussed in our previous study [14]. The detailed synthesis process, physical characterization and electrochemical characterization of CN_x nanofibers are also explained in the mentioned study [14]. It is shown that CN_x nanofibers showed excellent ORR catalytic activity comparable to Pt/C catalysts. In the present investigation to use CN_x nanofiber as cathode catalyst, the CN_x nanofiber deposited on Au metal is removed from the unwanted areas of the glass slide by lift-off using PG remover solution. Fig. 4 (a) and 4 (b) show the bright field image and dark field image of CN_x nanofibers on the Au surface after lift-off. Fig. 4 (c) and 4 (d) show bare Au and Pt as cathode respectively. It may be noted that electrospun CN_x nanofibers (Fig. 4 (e)) lost its nanofibrous morphology after lift-off (Fig. 4 (f)). PG remover, an organic solvent mixture composed of *N*-Methyl Pyrrolidinone (NMP), is used for lift-off. The loss in the nanofibrous shape of CN_x nanofibers is attributed to the solubility of PAN in NMP [19]. Fig. 4 (f) shows that Au surface consists of the uniformly distributed clusters. SEM image of the cluster (Fig. 4 (g)) shows that it consists of interconnected CN_x nanoparticles fused together. However, agglomeration of CN_x on a large scale is prevented as CN_x was dispersed in PAN nanofibers. As a result, the CN_x clusters individually are no bigger than 200 nm. The stability of CN_x on the gold surface is attributed to the binding property of Nafion® dispersion used as a filler in the CN_x nanofibers and the adhesive property of gold nanolayers deposited by EB evaporation system. In our earlier work [14], it is clearly shown that disintegrated CN_x nanofiber due to 5000 repetitive voltammetry became more stable and active towards ORR.

Fig. 5 (a) and 5 (b) shows the XPS wide scan spectrum of CN_x nanofibers before and after lift-off and Fig. 5 (c) and 5 (d) shows the corresponding N 1s spectrum. N percent in CN_x nanofibers reduces from 27% to 2% after lift-off is carried out which is because of removal of PAN nanofibers. The presence of F attributed to Nafion® in the wide scan spectrum of CN_x nanofibers after lift-off (Fig. 5 (b)) confirming that Nafion® aids in stabilization of CN_x clusters on gold nanolayers. The peak deconvolution of XPS of N1s core level spectra of CN_x nanofibers before and after lift-off is carried out based on the peak deconvulation carried out by Long et al. [20,21]. N1s spectrum of CN_x nanofibers before lift-off (Fig. 5 (c)) shows the presence of peaks at 398.3 eV and 398.9 eV, attributed to pyridinic N and nitrile N, respectively [22]. Pyridinic N, active species for ORR, is present due to the presence of CN_x nanoparticles and nitrile N due to PAN nanofibers. The removal of PAN after lift-off of CN_x nanofibers is confirmed by the absence of the peak at 398.9 eV in N 1s spectrum of CN_x nanofibers (Fig. 5 (d)).

Fig. 6 (a) shows the LSV plots of CN_x nanofibers and bare glassy

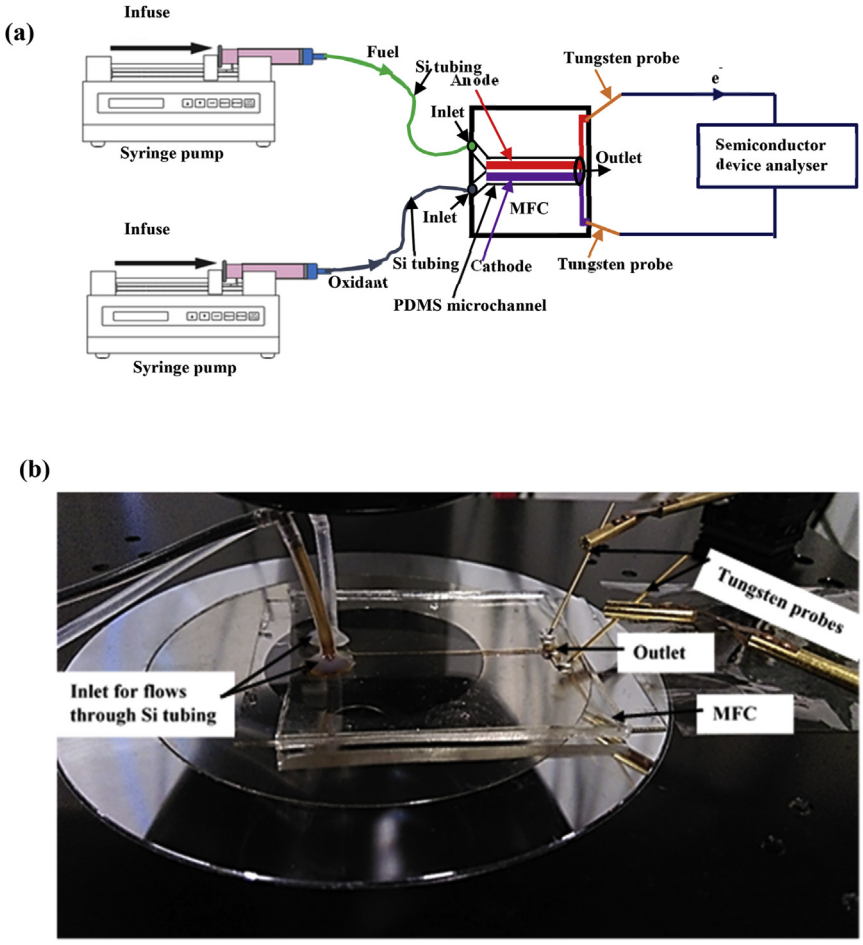

Fig. 3. (a) Schematic of microfluidic fuel cell during cell testing; (b) Actual photograph of microfluidic fuel cell experimental set-up.

carbon electrode towards $KMnO_4$ reduction, which display the reduction peak of CN_x nanofibers and glassy carbon electrode not active towards $KMnO_4$ reduction. Fig. 6 (a) shows that the onset potential and peak current density for $KMnO_4$ reduction of CN_x nanofibers is 1.5 V and 16.8 mA cm^{-2}, respectively. The observed values are improved as compared to onset potential of 0.95 V and peak current density of 6.32 mA cm^{-2} for ORR, as observed in our previous study [14], attributed to KMnO4 being a better cathodic electron acceptor than oxygen [17]. Fig. 6 (b) shows that CN_x nanofibers is stable in strong oxidative $KMnO_4$ condition with no change in peak current density and onset potential after 1000^{th} repetition. In order to study the crossover effect of formic acid fuel, LSV response is studied in $KMnO_4$ solution with and without 2.1 M HCOOH and is shown in Fig. 6 (c). The concentration of $KMnO_4$ taken is very low and the stoichiometry of the reaction between HCOOH and $KMnO_4$ is such that only 0.36 M HCOOH is consumed, which is negligible [23]. Similar voltammetry response to $KMnO_4$ reduction, with and without 2.1 M HCOOH, confirms that CN_x nanofibers is not active towards formic acid oxidation and is tolerant towards fuel crossover. Fig. 6 (c) shows no reduction peak when no $KMnO_4$ is added and only 0.5 M H_2SO_4 is used as the electrolyte confirming that $KMnO_4$ reduction is taking place at the electrode. The CV plots towards $KMnO_4$ reduction on Pt, Au and CN_x nanofibers are shown (Fig. S3) and explained in detail in the supplementary information. Briefly, CV plots confirm the presence of two reduction peaks corresponding to Mn (IV) to Mn (III) and Mn (III) to Mn (II). The reduction peak corresponding to Mn (IV) to Mn (III) is at 1.15 V, 1.1 V and 1.05 V for Pt, CN_x nanofibers and Au, respectively. Reduction peak for Mn (III) to Mn (II) at 0.6 V for Pt and Au is subdued as compared to CN_x nanofibers, suggesting that CN_x nanofibers has more electrocatalytic active surface for $KMnO_4$ reduction as compared to Pt and Au.

3.2. Flow behaviour and MFC operation

Flow rates of the fuel and the oxidant needs to be optimised in order to get maximum power density from the MFC. Importantly, anolyte and catholyte should mix minimum during its flow throughout the length of MFC. Fig. 7 (a) shows the variation of the interfacial width of the fuel and the oxidant flow in the microchannel for different flow rates at the middle and near the outlet of the microchannel. The coloured oxidant flow, that contains $KMnO_4$, enables the plotting of the flow profile at the interface through the microchannel based on the colour variation along the width of the microchannel. The snapshot of the microchannel, while the fluid flow is taking place, was taken using the CCD camera and the profile was plotted to measure the interfacial width using ImageJ software version 1.48 (NIH, USA). As an example, a snapshot of the microchannel at X = 36 mm for the flow rate of 300 μL min^{-1} is shown in Fig. 7 (b) and the corresponding profile is shown in Fig. 7 (c) (flow video is given in the supplementary information).

In order to get effective MFC power output, the interfacial width is needed to be less than the distance between the electrodes (100 μm), as shown by the black line in Fig. 7 (a). It is

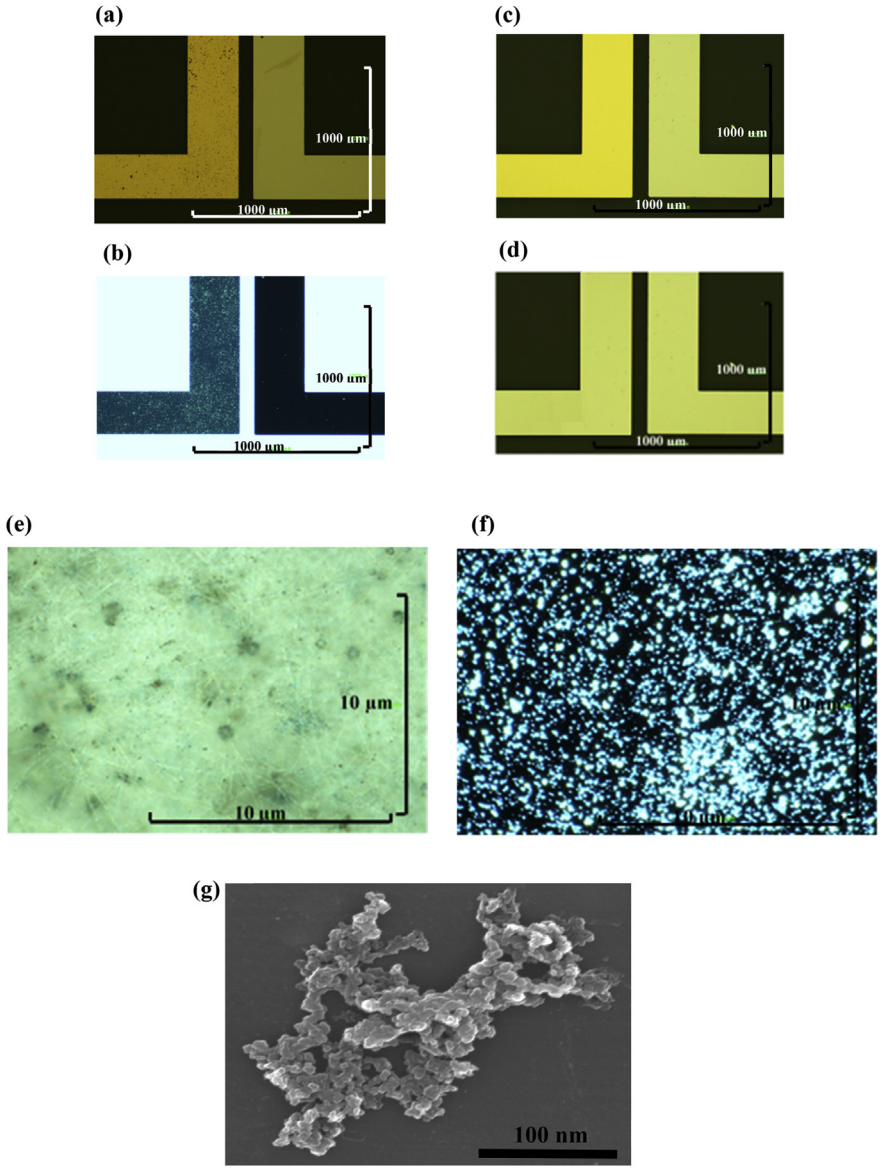

Fig. 4. Optical microscopic (a) bright field image and (b) dark field image of CN_x nanofibers as cathode catalyst on Au surface after lift-off. Bright field image of (c) bare Au and (d) Pt as cathode. Dark field image of CN_x nanofibers as cathode catalyst (e) before lift-off and (f) after lift-off; (g) SEM of a single cluster of CN_x catalyst after lift-off.

observed from the plot that the interfacial width is higher for low flow rates (50 µL min^{-1}, 100 µL min^{-1} and 200 µL min^{-1}), which is because of high diffusion rates. Since the interfacial width is more than 100 µm for 50 µL min^{-1} and 100 µL min^{-1}, the device fails as a fuel cell for these flow rates. For 200 µL min^{-1}, the interfacial width increasing along the length of the channel, which is equal to 100 µm near the outlet, making it infeasible to be used effectively as a fuel cell. The interfacial width reduces further with the increase in fluid flow rates. For higher flow rates of 400 µL min^{-1} and 500 µL min^{-1}, interfacial width is more near the outlet of the microchannel (85.1 µm and 80.9 µm, respectively) as compared to the middle of the microchannel (74.5 µm and 69.2 µm, respectively). The increase in interfacial width along the length of the microchannel at high flow rates is attributed to the low hydrodynamic stability of the anolyte and catholyte interface. The increase of the interfacial width along the length of the microchannel leads to high ohmic losses and consequently, low power density. Moreover, high flow rate leads to the low retention time of the fuel and low fuel efficiencies in the microchannel [6]. Increasing the fluid flow rate results in the oscillation of the interface causing hydrodynamic perturbation to such an extent that the fluid touched the opposite electrode leading to zero open circuit potential (OCP) beyond 500 µL min^{-1}. At the fluid flow rate of 300 µL min^{-1}, the interfacial width of the fluids is seen to be constant along the length of the microchannel (86 µm) and it is less than 100 µm. Thus 300 µL min^{-1} flow rate of anolyte and catholyte gives stable interface (<100 µm) with minimum flow rate. As a result, when the flow rates are decreased from 500 µL min^{-1} to 300 µL min^{-1}, the peak power density is increased from 2.44 mW cm^{-2} to 3.43 mW cm^{-2} for CN_x nanofibers (Fig. 8 (a)), from 2.23 mW cm^{-2} to 3.09 mW cm^{-2} for Pt (Fig. 8 (b)) and 1.81 mW cm^{-2} to 2.72 mW cm^{-2} for Au (Fig. 8 (c)).

In earlier studies [24], it is shown that the power density in MFC decreases with the decrease in fluid flow rate due to increase in the interfacial diffusion in the transverse direction of flow. Ahmed et al. [25] reported that the detrimental effect due to diffusion at the low

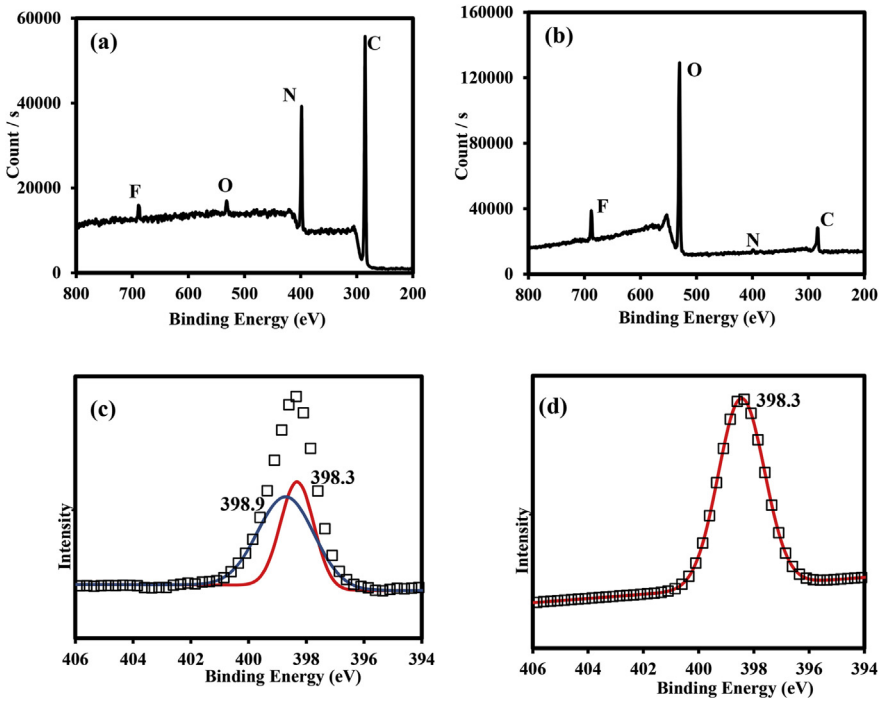

Fig. 5. XPS spectra of CN_x nanofibers: wide scan spectra (a) before lift-off, (b) after lift-off, N 1s core level spectra (c) before lift-off and (d) after lift-off.

flow rate may be overcome by increasing fuel utilization and bringing hydrodynamic stability, which would give rise to an improvement in MFC power density. Nasharudin et al. [26] argued that the crossover at lower flow rate is more because of diffusion compared to that due to hydrodynamic perturbations at higher flow rate. The dimensions of the flow architecture of MFC is such that the mean residence time of the fuel inside the microchannel (t) is negligible as compared to diffusion time (τ_D), the time required to mix anolyte and catholyte fully in the microchannel. Diffusion time is calculated as [27]:

$$\tau_D = \frac{W^2}{D} \quad (1)$$

where, W is the width of the microchannel (800 μm) and D is diffusivity of formic acid, calculated [28] as 1.19×10^{-9} m^2/s. Diffusion time (τ_D) is calculated as 538 s in the present case. Mean residence time (t) at a particular point in the downstream of the microchannel (X), depends on the height of the microchannel (H), width of the microchannel (W) and the flow rate of the fluid (Q) and it is calculated as:

$$t = \frac{X}{V_f} \quad (2)$$

where, V_f is the velocity of flow, which is given by,

$$V_f = \frac{Q}{H * W} \quad (3)$$

For flow rates of 300, 400 and 500 μL min^{-1}, velocity is calculated as 0.05, 0.067 and 0.083 m s^{-1}, respectively and the corresponding mean residence time is calculated as 0.7, 0.53 and 0.42 s near the outlet of the microchannel at X = 3.5 cm. The maximum value of mean residence time calculated, 0.7 s for 300 μL min^{-1}, is three orders of magnitude less than diffusion time, 538 s, confirming that the adverse effect of diffusion on power density at low flow rate is negligible. As a result of this, factors such as higher hydrodynamic instability and less fuel utilization leading to low power density is more dominant at higher flow rates. Consequently, the fuel crossover at high flow rates due to hydrodynamic perturbations is more than that at low flow rates due to diffusion. In Fig. 8 (b), there is a small kink for the flow rate of 500 μL min^{-1} at 0.5 V that resembles the passive region in a polarization curve, attributed to CO poisoning of the Pt cathode due to high fuel crossover. It is seen that the power density value decreases after 0.5 V at a constant current density. In Fig. 8 (c), OCP is seen to decrease from 1.1 V for 300 μL min^{-1} to 0.80 V for 500 μL min^{-1}. The reduction in OCP is attributed to high fuel crossover leading to reduced fuel and oxidant concentration along the length of the microchannel. The constant OCP in the polarization curves for CN_x nanofibers as cathode catalyst at different flow rates affirms suitability of CN_x catalyst to withstand fuel crossover as compared to Pt and Au. The suitability of CN_x nanofibers to withstand fuel crossover allows it to be operated with a wide range of flow rate of anolyte (formic acid) and catholyte (potassium permanganate). The absence of kink in the polarization curve of CN_x nanofiber is attributed to its ability to withstand CO poisoning due to its non-metallic nature as compared to Pt catalyst, as shown by Sun et al. [29]. It should be noted that CN_x is not active towards formic acid electrooxidation.

Fig. 8 (d) compares the MFC polarization curve at a flow rate of 300 μL min^{-1} for different cathode catalysts, e.g., CN_x nanofibers, Pt and Au. Table 1 summarizes the performance of MFC as shown in Fig. 8 (d). The flow videos of the fuel and the oxidant in the MFC that uses CN_x nanofibers, gold and platinum as cathode catalyst is shown in multimedia S4, S5 and S6 of the supplementary information, respectively. It is observed from multimedia S4, S5 and S6 that the flows are stable and the clear interface of the anolyte and catholyte is formed that lies within the 100 μm spacing between the electrodes. It is observed that when cathode catalyst is changed from Au to CN_x nanofibers, the peak power density increases from 2.72 mW cm^{-2} to 3.43 mW cm^{-2}, corresponding current density

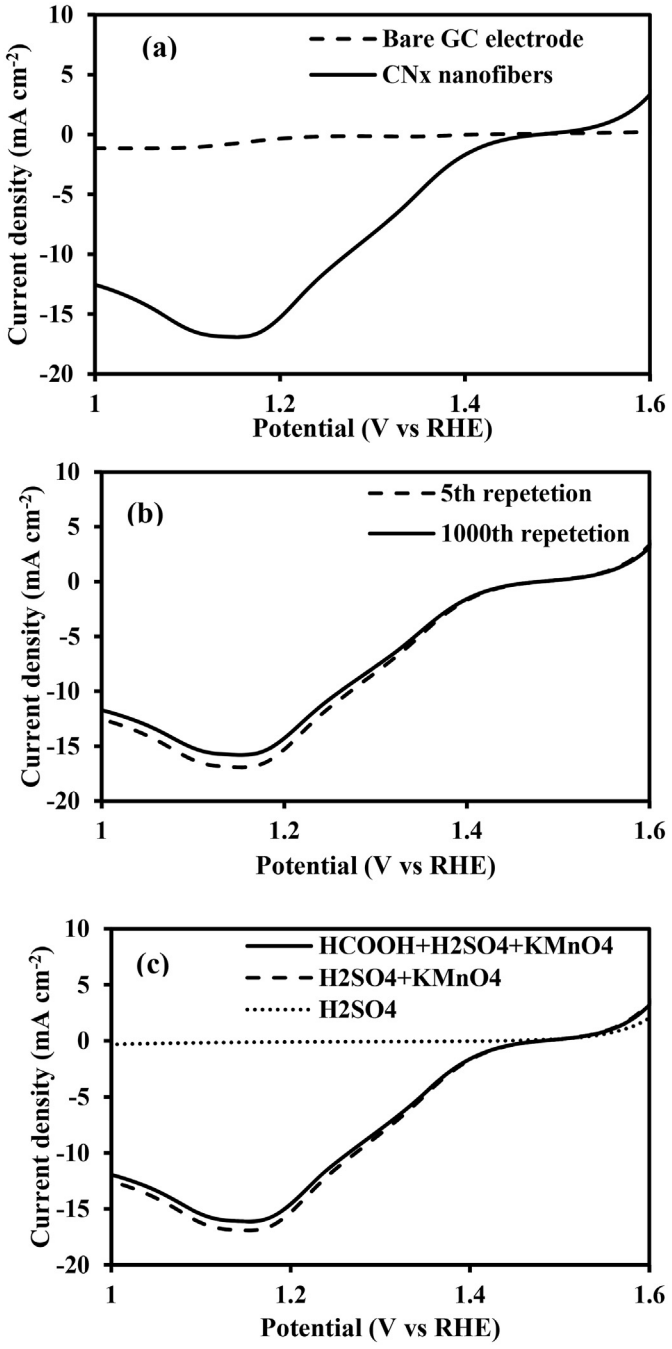

Fig. 6. Linear sweep voltammograms for $KMnO_4$ reduction: (a) CN_x nanofibers and bare glassy carbon electrode in 0.5 M H_2SO_4 + 0.144 M $KMnO_4$ solution, (b) CN_x nanofibers in 0.5 M H_2SO_4 + 0.144 M $KMnO_4$ solution at 5th and 1000th repetition, (c) CN_x nanofibers in 0.5 M H_2SO_4, 0.5 M H_2SO_4 + 0.144 M $KMnO_4$ and 0.5 M H_2SO_4 + 0.144 M $KMnO_4$ + 2.1 M HCOOH solutions to study HCOOH poisoning.

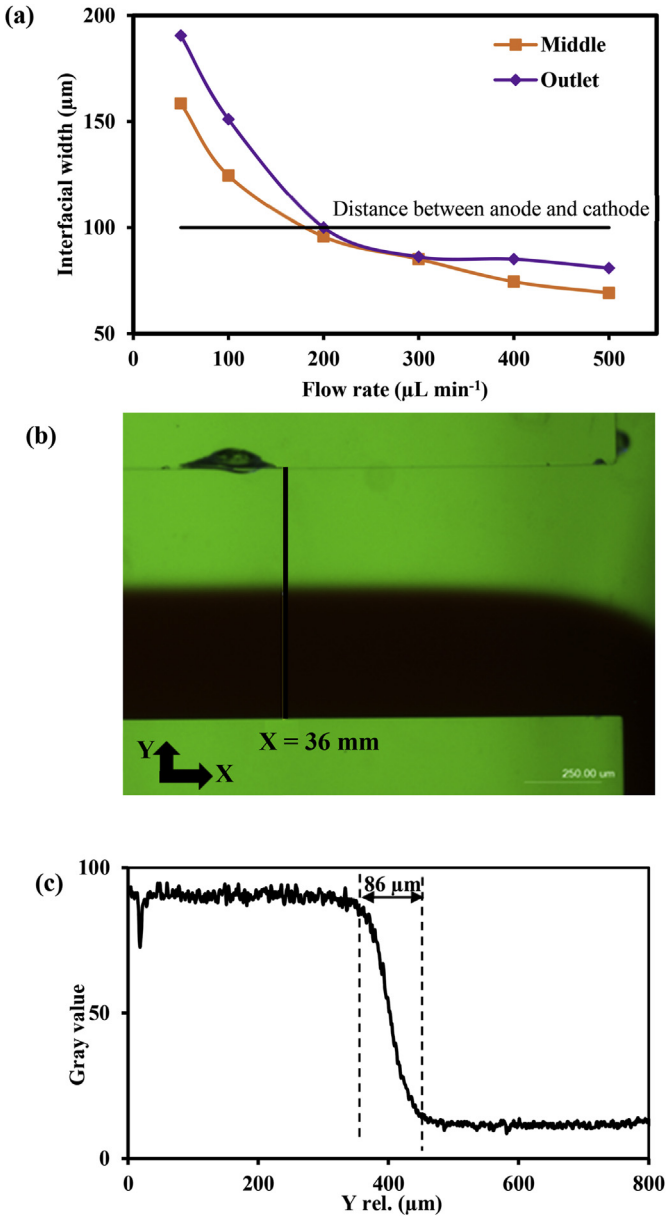

Fig. 7. (a) Width of the interface of the fuel and oxidant flow in the microchannel at different flow rates of the fluids at the middle (X = 18 mm) and near the outlet (X = 36 mm) of the microchannel. The black horizontal line indicates the distance between the electrodes; (b) Snapshot and (c) Plot profile of the microchannel near the outlet when fluid is flowing at the flow rate of 300 µL min^{-1}.

increases from 6.04 mA cm^{-2} to 9.79 mA cm^{-2}. CN_x nanofibers, as cathode catalyst, showed improved power density and current density as compared Pt cathode (power density: 3.09 mW cm^{-2} and current density: 6.18 mA cm^{-2}).

Supplementary video related to this article can be found at http://dx.doi.org/10.1016/j.jpowsour.2016.12.047.

4. Conclusions

MFC is fabricated using Y-shape PDMS microchannel aligned and soft bonded to metallized glass slides, which acted as anode and cathode with an active area of 0.11 cm^2. The use of CN_x nanofiber as cathode catalyst in MFC is demonstrated, which avoids the use of noble metal, allows the use of wide range of flow rates of anolyte (formic acid) and catholyte ($KMnO_4$) during MFC operation and is tolerant towards fuel crossover effect. MFC tested with CN_x nanofiber, Au and Pt as cathode catalysts give comparable OCP of 1.1 V and maximum power density and current density

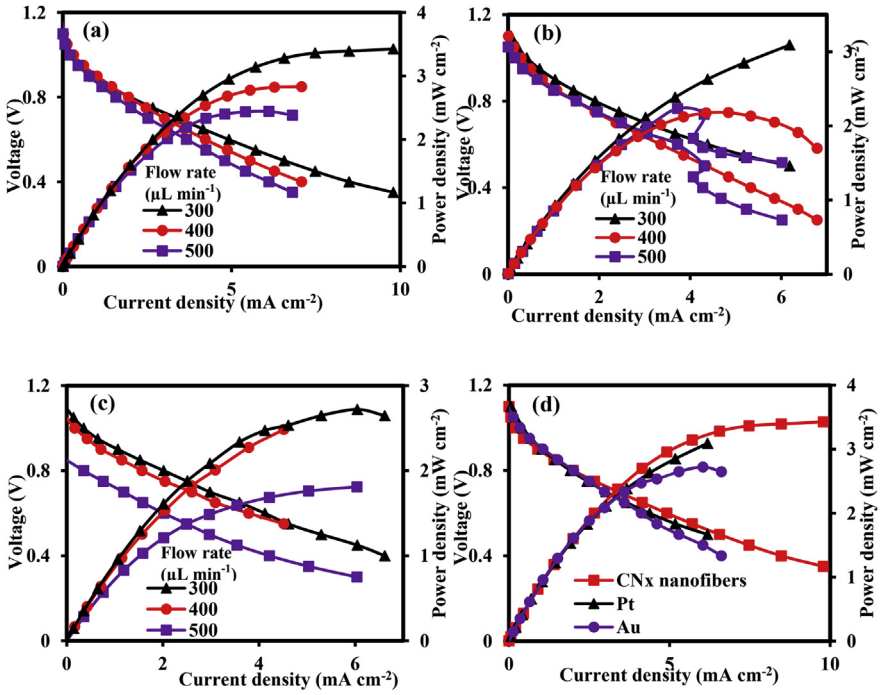

Fig. 8. Microfluidic fuel cell polarization curve and power density curve at different flow rates of 300, 400 and 500 μL min^{-1} with the cathode catalyst: (a) CN_x nanofibers, (b) Pt and (c) Au; (d) microfluidic fuel cell polarization curve and power density curve at flow rate of 300 μL min^{-1} for different cathode catalysts: CN_x nanofibers, Pt and Au.

Table 1
Performance characteristics of microfluidic fuel cell for different cathode catalysts (1 mg cm^{-2}, 50 nm); Anode: Pt (50 nm), Anolyte: 2.1 M HCOOH; Catholyte: 0.144 M $KMnO_4$; Supporting electrolyte: 0.5 M H_2SO_4.

Cathode catalyst	CN_x nanofibers	Pt	Au
Maximum power density (mW cm^{-2})	3.43	3.09	2.72
Current density (mA cm^{-2})	9.79	6.18	6.04
Open circuit potential (V)	1.1	1.1	1.05

(3.43 mW cm^{-2}, 9.79 mA cm^{-2}) for CN_x followed by Pt (3.09 mW cm^{-2}, 6.18 mA cm^{-2}) and Au (2.72 mW cm^{-2}, 6.04 mA cm^{-2}). The flow architecture of MFC is such that the diffusion of anolyte and catholyte through the interface is negligible at low flow rates. Contrary to previous studies, it is shown that lower flow rates, e.g., 300 μL min^{-1} gives maximum power density and current density in MFC.

Acknowledgements

Authors would acknowledge Department of Information Technology (DIT), Government of India for generous funding. Authors would acknowledge Dr. Yoshikata Nakajima, Bio-Nano Electronics Research Center, Toyo University, Japan for helping in carrying out i-V measurements for MFC using the semiconductor device analyser (Agilent Technology B1500A) and Prof. Toru Maekawa, Bio-Nano Electronics Research Center, Toyo University, Japan for his constant encouragement throughout the studies. Authors would acknowledge Indian Nanoelectronics User Program, Center for Nano Science and Engineering, IISc, Bangalore for carrying out initial MFC studies. The work has been conducted under BNERC, Toyo University-NRF, IIT Delhi joint research collaboration program.

Appendix A. Supplementary data

Supplementary data related to this article can be found at http://dx.doi.org/10.1016/j.jpowsour.2016.12.047.

References

[1] E.R. Choban, J.S. Spendelow, L. Gancs, A. Wieckowski, P.J.A. Kenis, Membraneless laminar flow-based micro fuel cells operating in alkaline, acidic, and acidic/alkaline media, Electrochim. Acta 50 (2005) 5390–5398.
[2] Q. Yi, H. Chu, M. Tang, Y. Zhang, X. Liu, Z. Zhou, et al., A novel membraneless direct hydrazine/air fuel cell, Fuel Cells 14 (2014) 827–833.
[3] A. Déctor, J.P. Esquivel, M.J. González, M. Guerra-balcázar, J. Ledesma-garcía, N. Sabaté, Formic acid microfluidic fuel cell evaluation in different oxidant conditions, Electrochim. Acta 92 (2013) 31–35.
[4] E. Kjeang, N. Djilali, D. Sinton, Microfluidic fuel cells : a review, J. Power Sources 186 (2009) 353–369.
[5] E.R. Choban, L.J. Markoski, A. Wieckowski, P.J.A. Kenis, Microfluidic fuel cell based on laminar flow, J. Power Sources 128 (2004) 54–60.
[6] S. Ali, M. Shaegh, N. Nguyen, S.H. Chan, A review on membraneless laminar flow-based fuel cells, Int. J. Hydrogen Energy 36 (2011) 5675–5694.
[7] K.S. Salloum, J.R. Hayes, C.A. Friesen, J.D. Posner, Sequential flow membraneless microfluidic fuel cell with porous electrodes, J. Power Sources 180 (2008) 243–252.
[8] M.H. Sun, G.V. Casquillas, Q. Ouyang, Y. Chen, Characterization of microfluidic fuel cell based on multiple laminar flow, Microelectron. Eng. 84 (2007) 1182–1185.
[9] A.S. Gago, D. Morales-acosta, L.G. Arriaga, N. Alonso-vante, Carbon supported ruthenium chalcogenide as cathode catalyst in a microfluidic formic acid fuel cell, J. Power Sources 196 (2011) 1324–1328.
[10] Y. Zheng, J. Liu, J. Liang, M. Jaroniec, S.Z. Qiao, Graphitic carbon nitride materials: controllable synthesis and applications in fuel cells and photocatalysis, Energy Environ. Sci. 5 (2012) 6717–6731.
[11] N. Daems, X. Sheng, I.F.J. Vankelecom, P.P. Pescarmona, Metal-free doped carbon materials as electrocatalysts for the oxygen reduction reaction, J. Mater. Chem. A 2 (2014) 4085–4110.
[12] S.M. Lyth, Y. Nabae, N.M. Islam, S. Kuroki, M. Kakimoto, S. Miyata, Electrochemical oxygen reduction activity of carbon nitride supported on carbon black, J. Electrochem. Soc. 158 (2011) B194–B201.
[13] A. Jindal, S. Basu, C.P. Aby, Electrospun carbon nitride supported on poly(vinyl) alcohol as an electrocatalyst for oxygen reduction reactions, RSC Adv. 5 (2015) 69378–69387.
[14] A. Jindal, S. Basu, Improvement in electrocatalytic activity of oxygen reduction reaction of electrospun carbon nitride/polyacrylonitrile nanofibers by addition of carbon black and nafion® fillers, Int. J. Hydrogen Energy 41 (2016)

11624–11633.
[15] A. Jindal, D.K. Gautam, S. Basu, Electrocatalytic activity of electrospun carbon nitride-polyacrylonitrile Nano fibre towards oxygen reduction reactions, J. Electroanal. Chem. 775 (2016) 198–204.
[16] W. Cai, L. Liang, Y. Zhang, W. Xing, C. Liu, Real contribution of formic acid in direct formic acid fuel cell : investigation of origin and guiding for micro structure design, Int. J. Hydrogen Energy 38 (2012) 212–218.
[17] S. You, Q. Zhao, J. Zhang, J. Jiang, S. Zhao, A microbial fuel cell using permanganate as the cathodic electron acceptor, J. Power Sources 162 (2006) 1409–1415.
[18] S. Ali, M. Shaegh, N. Nguyen, S.H. Chan, An air-breathing microfluidic formic acid fuel cell with a porous planar anode : experimental and numerical investigations, J. Micromechanics Microengineering 20 (2010) 105008.
[19] N. Oh, J. Jegal, K. Lee, Preparation and characterization of nanofiltration composite membranes using polyacrylonitrile (PAN). I. preparation and modification of PAN supports, J. Appl. Polym. Sci. 80 (2001) 1854–1862.
[20] G. Long, K. Wan, M. Liu, X. Li, Z. Liang, J. Piao, Effect of pyrolysis conditions on nitrogen-doped ordered mesoporous carbon electrocatalysts, Chin. J. Catal. 36 (2015) 1197–1204.
[21] G. Long, X. Li, K. Wan, Z. Liang, J. Piao, P. Tsiakaras, $Pt/C_{N\text{-}doped}$ electrocatalysts : superior electrocatalytic activity for methanol oxidation reaction and mechanistic insight into interfacial enhancement, Appl. Catal. B Environ. 203 (2017) 541–548.
[22] Z. Yue, K.R. Benak, J. Wang, L. Mangun, J. Economy, Elucidating the porous and chemical structures of ZnCl 2 -activated polyacrylonitrile on a fiberglass substrate, J. Mater. Chem. 15 (2005) 3142–3148.
[23] T. Lis, B. Jezowska-Trzebiatowska, The reaction between potassium permanganate and formic acid. Structural characterization of the polymeric compound $(K_2\{Mn(H_2O)_2[Mn_3O(HCOO)_9]_2\})_n$, Acta Crystallogr. Sect. B B33 (1977) 2112–2116.
[24] F. Chen, M. Chang, M. Lin, Analysis of membraneless formic acid microfuel cell using a planar microchannel, Electrochim. Acta 52 (2007) 2506–2514.
[25] D.H. Ahmed, H.B. Park, H.J. Sung, Optimum geometrical design for improved fuel utilization in membraneless micro fuel cell, J. Power Sources 185 (2008) 143–152.
[26] M.N. Nasharudin, S.K. Kamarudin, U.A. Hasran, M.S. Masdar, Mass transfer and performance of membrane-less micro fuel cell : a review, Int. J. Hydrogen Energy 9 (2014) 1039–1055.
[27] N. Miložič, M. Lubej, U. Novak, I. Plazl, Evaluation of diffusion coefficient determination using a microfluidic device, Chem. Biochem. Eng. Q. 28 (2014) 215–223.
[28] R.E. Treybal, Mass Transfer Operations, third ed., McGraw-Hill, New York, 1980.
[29] Y. Sun, C. Li, Y. Xu, H. Bai, Z. Yao, G. Shi, Chemically converted graphene as substrate for immobilizing and enhancing the activity of a polymeric catalyst, Chem. Commun. 46 (2010) 4740–4742.